

# Nonlinear dimensionality reduction of data by multilayer bootstrap networks

Xiao-Lei Zhang

**Abstract**—Learning invariant semantic concepts from highly-variant high-dimensional data is important in broad branches of science. If we encode the data and concepts compactly by for example 0 and 1, the golden pathway is a problem of reducing high-dimensional codes to low-dimensional representations. Dimensionality reduction, as a central problem of statistics and machine learning, has been intensively studied, where classification and clustering are two special cases of dimensionality reduction that reduce high-dimensional data to discrete points. Bootstrap resampling is a simple and fundamental method in statistics, and has achieved a great success in supervised dimensionality reduction. However, bootstrap based unsupervised dimensionality reduction methods were still not powerful compared to kernel methods and neural networks. Here we describe a simple multilayer bootstrap network for unsupervised dimensionality reduction that each layer of the network is a group of mutually independent k-centers clusterings, and the centers are only randomly sampled data points. We find that the described simple method outperformed 7 well-known unsupervised dimensionality reduction methods on both very small-scale biomedical data and large-scale image and document data with much less training time than multilayer neural networks on large-scale data. Our findings generalized bootstrap to unsupervised dimensionality reduction successfully and enriched the family of bootstrap methods. Furthermore, given the broad use of simple methods, the described method, which may be easily understood without domain knowledge, can find its applications in many branches of science.

**Index Terms**—Bootstrap methods, dimensionality reduction, ensemble methods, evolutionary computing, multilayer networks, kernel methods, sparse coding.

## I. INTRODUCTION

An excellent intelligent machine can at least learn the basic semantics of an objective, such as the disease types of a patient's DNA sequence, words of a handwritten or spoken sentence, and topics or sentiment of a story, without interfered by small variations of the objective. A common learning method is dimensionality reduction. The vitality of a dimensionality reduction method depends not only on its performance but also on how easily people in different areas can understand it, implement it, and use it. This paper focuses on unsupervised dimensionality reduction. A simple and widely used unsupervised method is principle component analysis (PCA), which finds a coordinate system that the linearly uncorrelated coordinate variables (called principle components) describe the most variances

of data. Because PCA is insufficient to capture highly-nonlinear data distributions, many nonlinear methods have been proposed.

Among the nonlinear methods, one prevalent class are nonparametric kernel (or graph) methods [1]–[9], which mainly keep the pairwise similarities of data points in the low-dimensional space as similar as possible as those in the original high-dimensional space. Because they need to calculate each pairwise similarity, their time and storage complexities scale squarely with the number of data points, limiting them to small-scale data. Another typical method is multilayer neural network [10]–[12], which gradually reduces the dimensionality of data through multiple layers of nonlinear transforms. It can handle large-scale problems well, but it is limited to large-scale problems and is difficult to be trained successfully with too many layers. Moreover, its structure and training method [11], [12] need careful manual-engineering, making it restricted to the experts of machine learning.

Besides, many machine learning techniques are doing dimensionality reduction (or approximation of data distribution) by either reducing the dimensionality of data explicitly or generating sparse high-dimensional features of data implicitly, such as probabilistic models [13]–[15] and sparse coding [16]. See [17], [18] for reviews of dimensionality reduction.

Bootstrap resampling [19], [20] is a simple and fundamental method in statistics and has achieved a great success in supervised dimensionality reduction, such as from logistic regression to adaptive boosting [21] and from regression tree to random forests [22]. However, bootstrap based unsupervised methods [23]–[25], which aggregate base predictions of a set of clusterings (see Supplementary Text), are still not strong enough compared to the state-of-the-art kernel methods or multilayer neural networks.

Here, we describe a very simple and robust multilayer bootstrap network (MBN) that can reduce the dimensions of both large-scale and small-scale data effectively and efficiently. MBN is trained simply by random sampling and nearest neighbor optimization under the basic idea that sampling a few data points from a local region is able to capture the manifold and meanwhile discard small variations of the region.

## II. ALGORITHM

MBN contains multiple hidden layers and an output layer (Fig. 1A). Each hidden layer is a group of mutually

The author is with Department of Computer Science and Engineering, The Ohio-State University, OH, USA, 43210.  
E-mail: huoshan6@126.com or xiaolei.zhang@gmail.com

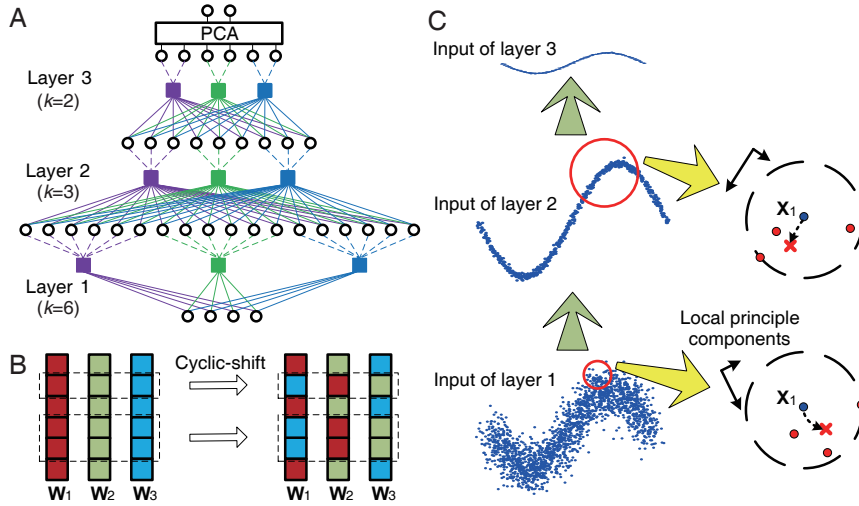


Fig. 1. Description of MBN. (A) The MBN network. Each square represents a  $k$ -centers clustering. (B) Random reconstruction. The columns represent the centers of a 3-centers clustering. Each square represents an entry of a center. (C) Principle of MBN. The regions in the red circles represent the local areas of the data point  $\mathbf{x}_1$ , which are further amplified in the dashed circles. Each red point in the dashed circle is the closest center of a  $k$ -centers clustering to  $\mathbf{x}_1$ . The new representation of  $\mathbf{x}_1$  in each layer is marked as a red cross in the dashed circle. The local principle components are shown in the upper and left corners of the dashed circles.

independent  $k$ -centers clusterings; each  $k$ -centers clustering has  $k$  output units, each of which indicates one cluster; the output units of all  $k$ -centers clusterings are concatenated as the input of their upper layer. The output layer is PCA. Parameter  $k$  should be as large as possible at the bottom layer and be smaller and smaller along with the increase of the number of layers.

MBN is trained layer-by-layer. For training each layer given a  $d$ -dimensional input data set  $\mathcal{X} = \{\mathbf{x}_1, \dots, \mathbf{x}_n\}$  either from the lower layer or from the original data space, we simply need to focus on training each  $k$ -centers clustering, which consists of four steps with the third step for small-scale problems only.

- **Random feature selection.** The first step randomly selects  $\hat{d}$ -dimensional features of  $\mathcal{X}$  ( $\hat{d} \leq d$ ) to form a subset of  $\mathcal{X}$ , denoted as  $\hat{\mathcal{X}} = \{\hat{\mathbf{x}}_1, \dots, \hat{\mathbf{x}}_n\}$ .
- **Random sampling.** The second step randomly selects  $k$  data points from  $\hat{\mathcal{X}}$  as the  $k$  centers of the clustering, denoted as  $\{\mathbf{w}_1, \dots, \mathbf{w}_k\}$ .
- **Random reconstruction.** When  $k$  approximates to  $n$  (i.e., the problem is small-scale), the third step randomly selects  $d'$  dimensions of the  $k$  centers ( $d' \leq \hat{d}/2$ ) and does one-step cyclic-shift as shown in Fig. 1B.
- **Sparse representation learning.** The fourth step assigns each input data point  $\hat{\mathbf{x}}$  to one of the  $k$  clusters and outputs a  $k$ -dimensional indicator vector  $\mathbf{h} = [h_1, \dots, h_k]^T$ , where operator  $T$  denotes the transpose of vector. For example, if  $\hat{\mathbf{x}}$  is assigned to the second cluster, then  $\mathbf{h} = [0, 1, 0, \dots, 0]^T$ . The assignment is calculated according to the similarities between  $\hat{\mathbf{x}}$  and the  $k$  centers, in terms of some predefined similarity measurement at the bottom layer, such as the Euclidean distance  $\arg \min_{i=1}^k \|\mathbf{w}_i - \hat{\mathbf{x}}\|^2$ , or in terms of  $\arg \max_{i=1}^k \mathbf{w}_i^T \hat{\mathbf{x}}$  at all other hidden layers.

TABLE I  
DESCRIPTION OF PARAMETERS.

Parameter	Description
$n$	Number of data points in the training set
$d$	Dimension of data
$s$	Sparsity of data, i.e. the fraction of the number of nonzero elements over all elements of data
$L$	Number of layers of MBN
$V$	Number of $k$ -centers clusterings per layer in MBN
$k$	Number of centers per clustering in MBN. Note that the clusterings in the same layer have the same number of centers
$a$	Fraction of the randomly selected features (i.e. $\hat{d}$ ) over all input features (i.e. $d$ ) in MBN
$r$	Fraction of the randomly shifted features (i.e. $d'$ ) over all features of the centers (i.e. $\hat{d}$ ) in the random reconstruction operation of MBN

MBN handles large-scale problems well. For training each layer, the time complexity is  $O(nsk^2V^2)$ , and the storage complexity is  $O(2nskV)$ , where  $V$  is the number of clusterings and  $s$  the sparsity of the input data (i.e., the ratio of the non-zero elements over all elements); particularly,  $s = 1/k$  (see Supplementary Text for detailed complexity analysis and Table I for the description of the parameters).

### III. THEORETICAL JUSTIFICATION

MBN has a simple geometric explanation. It first conducts piecewise-linear dimensionality reduction—a local PCA that gradually enlarges the area of local regions (Fig. 1C)—implicitly in hidden layers, and then gets low-dimensional features explicitly by PCA. Specifically, each data point (e.g.,  $\mathbf{x}_1$  in Fig. 1C) owns a local region supported by the centers of all clusterings that are closest to the data point. The centers define the local coordinate system. The new representation of the data point is the

coordinates of the data point in the local coordinate system. If some other data points share the same local region, they will also be projected to the same coordinates, which means the small variances (i.e., small principle components) of this local region that are not covered by the local coordinate system will be discarded. It is easy to image that when  $k$  is smaller and smaller, the local region is gradually enlarged, making larger and larger relatively-unimportant local variances discarded. However, when  $k$  approximates to  $n$ , the area of most local regions are zero, resulting in no approximations (i.e., dimensionality reductions) in these regions. To prevent this unwanted situation, we borrowed the reconstruction step (a.k.a., crossover) of genetic algorithm [26]. After random reconstruction, the centers not only will not appear in the input data but also can still define the coordinate systems of the local data distributions.

Besides the geometric explanation, MBN is also rooted in the bootstrap theory and regularization theory from the statistics and machine learning perspectives. (i) According to the theories of bootstrap resampling [19], [20], [27], weak learnability [28], and ensemble learning [22]–[24], [29]–[32], MBN is a stack of bootstrap resampling or clustering ensembles: a) each  $k$ -centers clustering is a bootstrap sample or a weak learner that is slightly better than random guess; multiple clusterings group to a strong learner that reduces the variances of local regions effectively. b) Because random sampling on small-scale data sets will cause clusterings overfit data, we borrowed the reconstruction step of genetic algorithm [26] to further process sampled data so as to not only prevent overfitting but also enlarge the diversity between the clusterings. (ii) According to the theory of regularization [33]–[35], MBN is a stack of regularization networks: each  $k$ -centers clustering is a  $\ell_\infty$ -norm-regularized network; motivated by the margin explanation of adaptive boosting on Vapnik-Chervonenkis dimension [21], [36]–[38], we proved that learning a group of  $k$ -centers clusterings is a sparse coding that is lower bounded by  $\ell_1$ -norm-regularized sparse coding [16] (see Theorem 1).

Different from the above theoretical base, MBN was motivated from (i) *product of experts* (PoE) [39], [40] and deep belief network (DBN) [15], (ii) factorization of restricted Boltzmann machine (RBM) [12], [15] (the building block of DBN) and contrastive divergence learning [40], and (iii) our theoretical proof on the relationship between PoE and sparse coding [16], [41] (see Theorem 1) and empirical results of sparse coding in [41]. Our motivation and derivation are as follows.

#### A. Relationship to product of experts

PoE aims to combine multiple individual models by multiplying them, where the individual models have to be a bit more complicated and each contains one or more hidden variables [40]. Its general probability framework is:  $p(\mathbf{x}) = \prod_{v=1}^V g_v(\mathbf{x}) / \sum_{\mathbf{x}'} \prod_{v=1}^V g_v(\mathbf{x}')$ , where  $\mathbf{x}'$  indexes all possible vectors in the data space, and  $g_v$  is called an *expert*. It is originally proposed to deal with the curse of

dimensionality. Specifically, a function that can be fully expressed by a *mixture of experts* with  $N$  experts (i.e. mixtures), such as Gaussian mixture model or  $k$ -means clustering, can be expressed compactly by a PoE with only  $\log_2 N$  experts [42]. Due to such a compact expression, given the same number of experts, a product of experts can be exponentially powerful than a mixture of experts.

RBM is a representative of PoE that each expert contains only one hidden variable, which yields the most compact representation. For example, the expert of Bernoulli-Bernoulli RBM is specified as  $g_v(\mathbf{x}) = \sum_{h_v \in \{0,1\}} \exp(c_v h_v + h_v \mathbf{W}_{v,:} \mathbf{x})$  where  $h_v \in \{0,1\}$  is a binary hidden variable, and  $\{c_v, \mathbf{W}_{v,:}\}$  are the parameters of the  $v$ -th expert. However, because RBM pursues the most compact expression too much, it loses the merit of the *explaining away* property, which performs like an information filter that discards the variations of input but only preserves manifold information. It is easy to observe that (i) to obtain the explaining away property, each expert needs at least two hidden units, one activated and the other inactivated, and (ii) one-hot encoding [42] (a.k.a. 1-of- $k$  encoding [43]) based hard-clustering, such as  $k$ -means, is one of the simplest experts that own the explaining away property. Based on the above analysis, we generalized the most compact PoE to a PoE whose expert owns multiple hidden units.

#### B. Relationship to contrastive divergence learning

Contrastive divergence learning is a  $t$ -step ( $t \geq 1$ ) approximation of maximum likelihood learning that originally aims to train RBM by the full Markov-chain Monte Carlo sampling [44]. Specifically, because RBM can be factorized to a serial binary-class experts given the input and vice versa, it trains each expert in each step separately. Because training each expert to be a very strong one via the full Markov-chain Monte Carlo sampling is quite inefficient, RBM trains each expert just stronger than random guess.

Motivated by the above, we adopted  $k$ -means clusterings with the expectation-maximization optimization [43] as experts, each of which has  $k$  output units. Because expectation-maximization is very expensive, particularly when  $k$  is large. We proposed to discard expectation-maximization completely but only preserve random sampling as a good initialization for training each expert, which is the bootstrap resampling. Theoretically, when  $k$  is large enough, a bootstrap sample can approximate data distribution correctly, hence, pursuing the center of each local region is statistically meaningless—using bootstrap resampling is enough to establish a strong learner.

#### C. Relationship to sparse coding

Given a learned dictionary  $\mathbf{W}$ , sparse coding typically aims to solve  $\min_{\mathbf{h}_i} \sum_{i=1}^n \|\mathbf{x}_i - \mathbf{W}\mathbf{h}_i\|_2^2 + \lambda \|\mathbf{h}_i\|_1$ , where  $\|\cdot\|_q$  represents  $\ell_q$ -norm,  $\mathbf{h}_i$  is the sparse code of the data point  $\mathbf{x}_i$ , and  $\lambda$  is a hyperparameter controlling the sparsity of  $\mathbf{h}_i$ . Each column of  $\mathbf{W}$  is called a basis vector. We may also view  $\lambda$  as a hyperparameter that controls the number

of clusterings. Specifically, if we set  $\lambda = 0$ , it is likely that  $\mathbf{h}_i$  contains only one nonzero element. Intuitively, we can understand it as that we use only one clustering to learn a sparse code. A good value of  $\lambda$  can make a small part of the elements of  $\mathbf{h}_i$  nonzero. This choice approximates to the method of partitioning the dictionary to several (probably overlapped) subsets and then grouping the basis vectors in each subset to a base clustering.

Empirically, Coates and Ng [41] conducted a broad experimental comparison on sparse coding, and observed that using random sampling to form a dictionary and using *soft threshold* to extract sparse features can be highly competitive to complicated sparse coding methods. Because the method in [41] can be regarded as a single  $k$ -centers clustering that uses a few nearest centers of a data point as the nonzero elements of the output sparse code of the data point. As a mixture of experts, the method in [41] is less effective than the building block of MBN theoretically.

To summarize, we prove the theoretical relationship between PoE, sparse coding, and each layer of MBN formally as follows:

*Theorem 1:* Each layer of MBN is a PoE whose experts are formulated as  $k$ -centers clusterings. It is lower bounded by  $\ell_1$ -norm sparse coding when given the same dictionary.

*Proof:* PoE maximizes the likelihood of the following equation:

$$p(\mathbf{x}) = \frac{\prod_{v=1}^V g_v(\mathbf{x})}{\sum_{\mathbf{x}'} \prod_{v=1}^V g_v(\mathbf{x}')} \quad (1)$$

Here we formulate  $g_v(\mathbf{x})$  as a  $k$ -means clustering with Euclidean distance as the similarity metric:

$$g_v(\mathbf{x}) = \mathcal{MN}(\mathbf{x}; \mathbf{W}_v \mathbf{h}_v, \sigma^2 \mathbf{I}) \quad (2)$$

subject to  $\mathbf{h}_v$  is a one-hot code

where  $\mathcal{MN}$  denotes the multivariate normal distribution,  $\mathbf{W}_v = [\mathbf{w}_{v,1}, \dots, \mathbf{w}_{v,k}]$  is the weight matrix whose columns are centers,  $\mathbf{I}$  is the identity matrix, and  $\sigma \rightarrow 0$ .

Given a data set  $\{\mathbf{x}_i\}_{i=1}^n$ . Substituting Eq. (2) to Eq. (1) and taking the negative logarithm of Eq. (1) derives the following problem:

$$\min_{\{\{\mathbf{h}_{v,i}\}_{i=1}^n\}_{v=1}^V} \sum_{v=1}^V \sum_{i=1}^n \|\mathbf{x}_i - \mathbf{W}_v \mathbf{h}_{v,i}\|_2^2, \quad (3)$$

subject to  $\mathbf{h}_{v,i}$  is a one-hot code.

If we denote  $\mathbf{W} = [\mathbf{W}_1, \dots, \mathbf{W}_V]$  and further complement the head and tail of  $\mathbf{h}_{v,i}$  with multiple zeros, denoted as  $\mathbf{h}'_{v,i}$ , such that  $\mathbf{W} \mathbf{h}'_{v,i} = \mathbf{W}_v \mathbf{h}_{v,i}$ , we can rewrite Eq. (3) to the following equivalent problem:

$$\min_{\{\{\mathbf{h}_{v,i}\}_{i=1}^n\}_{v=1}^V} \sum_{v=1}^V \sum_{i=1}^n \|\mathbf{x}_i - \mathbf{W} \mathbf{h}'_{v,i}\|_2^2, \quad (4)$$

subject to  $\mathbf{h}_{v,i}$  is a one-hot code.

It is an integer optimization problem that has an integer matrix variable  $\mathbf{H}'_v = [\mathbf{h}'_{v,1}, \dots, \mathbf{h}'_{v,n}]$ . Suppose there are totally  $|\mathcal{H}'_v|$  possible solutions of  $\mathbf{H}'_v$ , denoted as  $\mathbf{H}'_{v,1}, \dots, \mathbf{H}'_{v,|\mathcal{H}'_v|}$ , we first relax Eq. (4) to a convex

optimization problem by constructing a *convex hull* [45] on  $\mathbf{H}'_v$ :

$$\min_{\{\{\mu_{v,k}\}_{k=1}^{|\mathcal{H}'_v|}\}_{v=1}^V} \sum_{v=1}^V \sum_{i=1}^n \left\| \mathbf{x}_i - \mathbf{W} \left( \sum_{k=1}^{|\mathcal{H}'_v|} \mu_{v,k} \mathbf{h}'_{v,k,i} \right) \right\|_2^2 \quad (5)$$

subject to  $0 \leq \mu_{v,k} \leq 1, \sum_{k=1}^{|\mathcal{H}'_v|} \mu_{v,k} = 1,$   
 $\forall v = 1, \dots, V.$

Because Eq. (5) is a convex optimization problem, according to Jensen's inequality, the following problem learns a lower bound of Eq. (5):

$$\min_{\{\{\mu_{v,k}\}_{k=1}^{|\mathcal{H}'_v|}\}_{v=1}^V} V \sum_{i=1}^n \|\mathbf{x}_i - \mathbf{W} \mathbf{h}_i''\|_2^2 \quad (6)$$

subject to  $0 \leq \mu_{v,k} \leq 1, \sum_{k=1}^{|\mathcal{H}'_v|} \mu_{v,k} = 1,$   
 $\forall v = 1, \dots, V.$

where  $\mathbf{h}_i'' = \frac{1}{V} \sum_{v=1}^V \sum_{k=1}^{|\mathcal{H}'_v|} \mu_{v,k} \mathbf{h}'_{v,k,i}$  with  $\mu_{v,k}$  as a variable.

Recalling the definition of sparse coding given a fixed dictionary  $\mathbf{W}$ , we observe that Eq. (6) is a special form of sparse coding with more strict constraints on the format of sparsity.

Therefore, given the same dictionary  $\mathbf{W}$ , when the experts of PoE are formulated as  $k$ -means clustering, PoE is a distributed sparse coding that is lower bounded by the common  $\ell_1$ -norm sparse coding.

When we discard the expectation-maximization optimization of each  $k$ -means clustering (i.e., dictionary learning) but only preserve the default initialization method – random sampling, Eq. (1) becomes the building block of MBN. Given the same dictionary,  $\ell_1$ -norm-regularized sparse coding is a convex relaxation of the building block of MBN. Theorem 1 is proved. ■

#### IV. SUMMARY OF EMPIRICAL STUDY

To demonstrate the effectiveness of MBN on small-scale data sets, we compared MBN with PCA and 4 well-known nonlinear dimensionality reduction methods, including isometric feature mapping (Isomap) [3], locally linear embedding (LLE) [4], spectral clustering (Spectral) [5], and  $t$ -distributed stochastic neighbor embedding (t-SNE) [9], on the acute myeloid leukemia (AML) and acute lymphoblastic leukemia (ALL) biomedical data which consist of only 38 training examples and 34 test examples [46] (see Materials and Methods). Because multilayer neural network cannot handle such a small-scale data set, we will not compare with it. We produced low-dimensional features of the data set for visualization (Fig. 2A) and clustering (Fig. 2B). Clustering accuracy was measured by the normalized mutual information [23]. Experimental results show that MBN outperformed the referenced methods on both visualization and clustering accuracy.

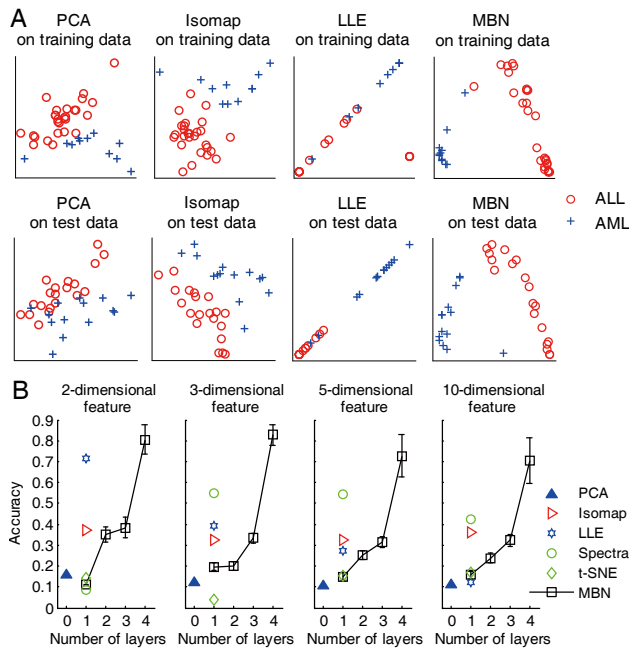


Fig. 2. Reducing the dimensionality of the 7,129-dimensional AML-ALL biomedical data which consist of 72 examples. (A) Visualizations produced by PCA, Isomap, LLE, and MBN at layer 4 respectively. Visualizations produced by other layers of MBN are shown in fig. S1 in the Supplementary Materials. (B) Accuracy comparison of the  $k$ -means clusterings using the low-dimensional features produced by MBN and 5 competitive methods respectively.

We also compared MBN with the aforementioned 5 referenced methods and DBN [12], a multilayer neural network with stacked RBM [15] as the initialization, on small subsets of the MNIST handwritten digits [47], each of which consists of 5,000 images (see Materials and Methods). Experimental results show that (i) MBN achieved an ideal visualization of the 10 digits and outperformed other referenced methods; (ii) although t-SNE also achieved a clear visualization, the visualization produced by MBN had larger between-class distances and smaller within-class variations (i.e., clearer visualization when we do not draw colors on the digits) than that produced by t-SNE (Fig. 3A). When the low-dimensional features were applied for clustering, MBN reached an accuracy of about 82.3% while the best competitor reached about 77.5% (Fig. 3B).

To investigate the scalability and effectiveness of MBN on large-scale problems, we compared MBN with PCA and DBN on the full MNIST handwritten digits [47] which consist of 60,000 training images and 10,000 test images (see Materials and Methods). Because Isomap, LLE, Spectral, and t-SNE cannot handle such a large-scale problem, we did not compare with them. Experimental results show that MBN achieved a clear visualization on the 10 digits (Fig. 4A) with a limited computational budget. When the low-dimensional features were applied for clustering, MBN was as good as DBN when they had the same number of layers, and outperformed DBN when more layers were easily stacked (Fig. 4B). When the experiment was run on a one-core personal computer, MBN consumed one-order

less training time than DBN (Fig. 4C).

We also compared MBN with DBN and latent semantic analysis (LSA) [48], a well-known document retrieval method based on PCA, on a larger data set—Reuters newswire stories [49] which consist of 804,414 documents with half of the documents used for training and the other half for test (see Materials and Methods). Experimental results show that MBN achieved a clear visualization on 9 demo topics (Fig. 5A). When the documents were reduced to five-dimensional features for document retrieval, MBN reached an accuracy of about 10% higher than LSA when only a handful of documents were retrieved, and this superiority was enlarged slightly when more documents were retrieved (Fig. 5B). When the experiment was run on a one-core personal computer, MBN was faster than DBN on the training time (Fig. 5C).

Besides the above empirical comparisons, we further analyzed the impacts of different parameter settings of MBN on performance (see Materials and Methods). Experimental results show that (i) fortunately, the time complexity scaled linearly but not squarely with  $V$ , which can only be explained as that the input features of each layer were sparse (Fig. 6); (ii) the performance was robust to different parameter settings (Figs. 7 to 10). The detailed evolving process of MBN on ALL-AML, MNIST, and Reuters newswire stories are shown in Supplementary Materials.

## V. DISCUSSIONS

In this paper, we have proposed multilayer bootstrap networks for nonlinear dimensionality reduction. MBN has a novel network structure that each expert is a  $k$ -centers clustering whose centers are only randomly sampled data points. To prevent overfitting, MBN also uses a cyclic-shift to randomly reconstruct the centers. Its time and storage complexities scale linearly with the size of training data. It is quite easily understood, implemented, and used, even without the knowledge of machine learning. It performs robustly with different parameter settings. It supports parallel computing naturally. Empirical results demonstrated its effectiveness and efficiency.

Theoretically, MBN extended bootstrap resampling methods [19]–[21], [27], [28] to an unsupervised multilayer architecture and borrowed evolutionary computing [26] to prevent overfitting. Compared to learning with kernels [1], [2], [5], [37], [38], [50], MBN scales linearly with the size of datasets, which overcomes the fundamental weakness of learning with kernels. Compared to neural networks [11], [12] which minimizes empirical risk with many bad local minima, MBN minimizes structural risk [38] under the smooth assumption that a small variation on the input data results in only a small variation on the output target [34], such that it performs well not only on large-scale data but also on very small-scale data. Finally, as a successful method for unsupervised learning, multilayer bootstrap networks enriched the family of bootstrap methods [19], [20].

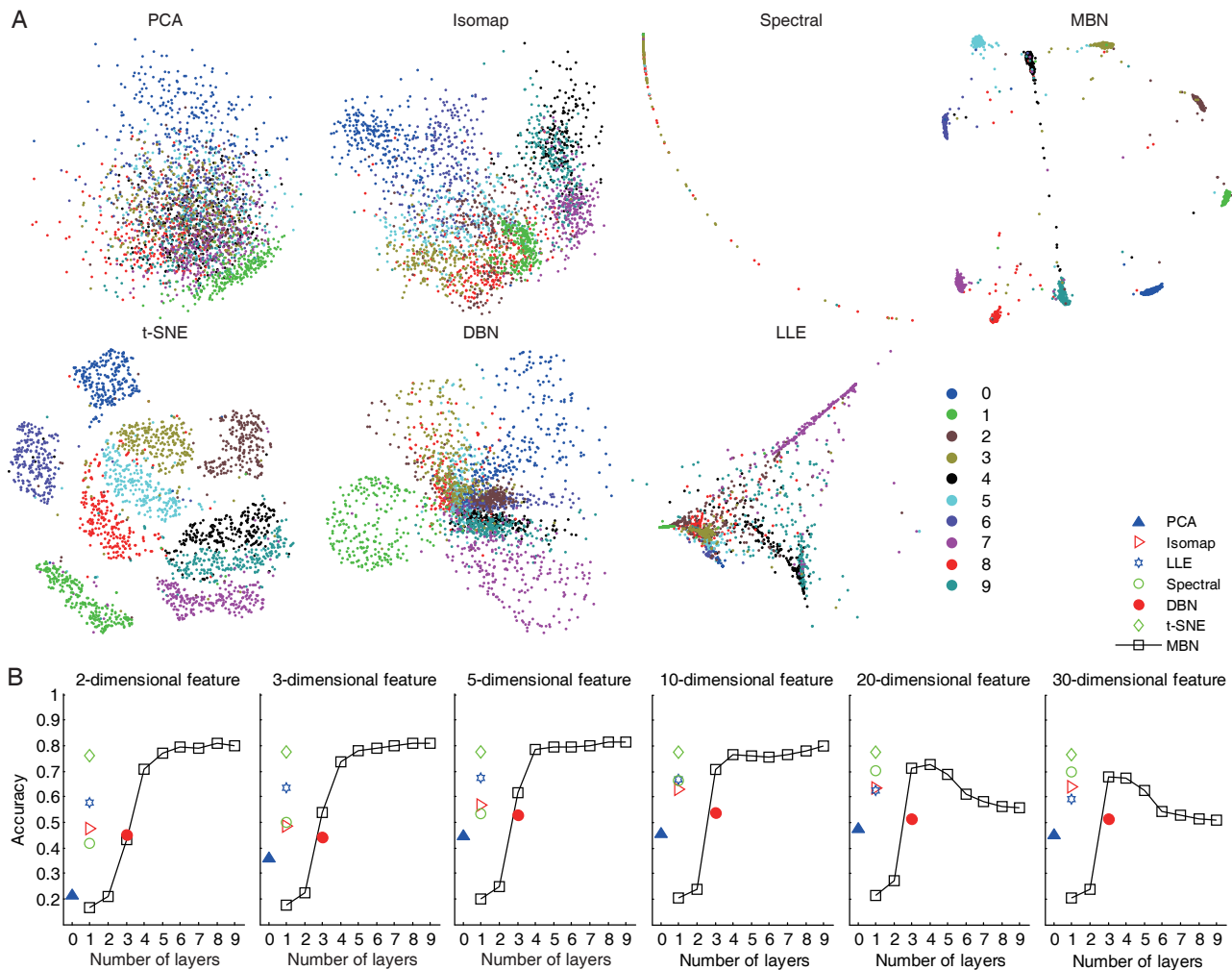


Fig. 3. Reducing the dimensionality of subsets of the 784-dimensional MNIST handwritten digits, each of which consists of 5,000 images. (A) Visualizations produced by 6 competitive methods and MBN at layer 7. For clarity, only 250 images per digit are drawn. Visualizations produced by other layers of MBN are shown in fig. S2 in Supplementary Materials. (B) Accuracy comparison of the  $k$ -means clusterings using the low-dimensional features produced by MBN and 6 competitive methods respectively.

## VI. MATERIALS AND METHODS

### A. Detailed Implementation of MBN

When a data set was small-scale, we used the linear-kernel-based kernel PCA [51], [52] as the PCA toolbox. When the data set was middle- or large-scale, we used the expectation-maximization PCA (EM-PCA) [53] as the PCA toolbox. Kernel PCA can handle a data set that the dimension of the data points is larger than the size of the data set, but its time and storage complexities scale squarely with the size of the data set. EM-PCA can handle large-scale and high-dimensional problems efficiently, but it suffers from local minima. When we used the low-dimensional features for clustering, the  $k$ -means clustering algorithm was an implementation in VOICEBOX [54].

### B. Experimental Platform

All experiments were run with the Matlab2012b software. When we evaluated the accuracy, MBN was run with at most 72 central processing units (CPUs) launched by

the parallel computing toolbox of Matlab in the Ohio Supercomputing Center, OH, USA, where each CPU trained one  $k$ -centers clustering at a time. When we evaluated the training time, all competitive methods were run with one-core personal computer with 8 GB memory. Only the CPU time consumed on dimensionality reduction was recorded.

### C. Parameter Notations

MBN has four key parameters: (i) parameter  $V$  denotes the number of  $k$ -centers clusterings per layer; (ii) parameter  $k$  denotes the number of the output units of a  $k$ -centers clustering; (iii) parameter  $a$  denotes the fraction of the randomly selected features (i.e.  $\hat{d}$ ) over all input features (i.e.  $d$ ); (iv) parameter  $r$  denotes the fraction of the shifted features (i.e.  $d'$ ) over all features of the centers (i.e.  $\hat{d}$ ) in the random reconstruction operation. Besides, the user has to define the similarity measurement of the bottom layer. The commonly used measurements are Euclidean distance and linear kernel. We summarized the hyperparameters in Table 1.

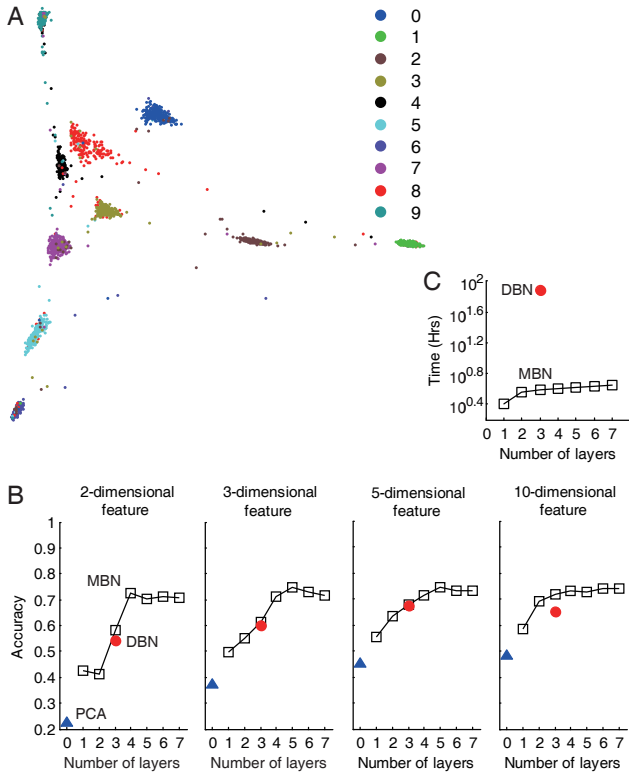


Fig. 4. Reducing the dimensionality of the 784-dimensional MNIST handwritten digits which consist of 70,000 images. (A) Visualization of MNIST produced by MBN at layer 7. For clarity, only 250 images per digit are drawn. Visualizations produced by other layers are similar to fig. S2 in Supplementary Materials. We also provided visualizations of MBN without random reconstruction in fig. S3 in Supplementary Materials. (B) Accuracy comparison of the  $k$ -means clusterings using the low-dimensional features produced by MBN, PCA and DBN respectively on the 10,000 test images. (C) Training time (in hours) comparison between MBN and DBN on MNIST.

#### D. Experimental Details on the AML-ALL Biomedical Data

The AML-ALL biomedical data set [46], [55] is a two-class classification problem that consists of 38 training examples (27 ALL, 11 AML) and 34 test examples (20 ALL, 14 AML). Each example has 7,129 dimensions produced from 6,817 human genes. The smallest value and largest value of the data are  $-28400$  and  $71369$  respectively. We normalized the data to the range  $[0, 1]$  by preprocessing each entry of the data  $x$  by  $(x + 28400)/(71369 + 28400)$ . Note that MBN did not have to use the normalized data. The normalization was mainly for a fair comparison with the competitive methods that had to use the normalized data. It is also a common preprocessing method for preventing the numerical computing error of computer.

The parameter setting of MBN was as follows. The number of hidden layers was set to 4. Parameters  $k$  from layer 1 to layer 4 were set to 30-15-8-4 respectively. Parameter  $V$  was set to 2000 for all layers. Parameter  $a$  was set to 0.5. Parameter  $r$  was set to 0.5. The output dimension of the linear-kernel-based kernel PCA was selected from  $\{2, 3, 5, 10\}$ . Euclidean distance was used as the similarity measurement of the bottom layer.

We compared MBN with PCA, Isomap [3], LLE [4],

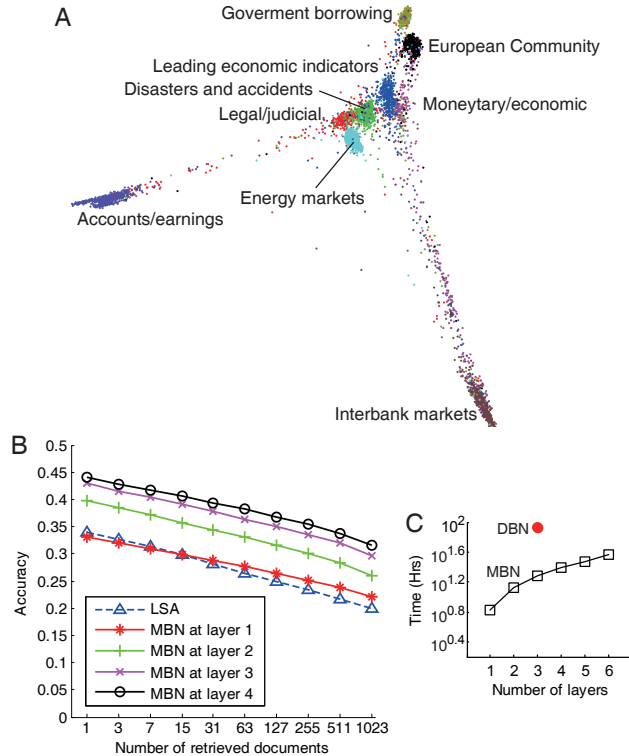


Fig. 5. Reducing the dimensionality of the 2,000-dimensional Reuters newswire stories which consist of 804,414 documents. (A) Visualization of 9 demo topics of the Reuters newswire stories produced by MBN at layer 6. For clarity, only 500 documents per topic are drawn. Visualizations produced by other layers of MBN are shown in fig. S4 in Supplementary Materials. (B) Average accuracy curves of retrieved documents over 402,207 queries (including 82 topics) on the test set of the Reuters newswire stories produced by MBN and LSA. Each query is a 5-dimensional document from the test set. The accuracy is defined as the proportion of the retrieved documents that are in the same class as the query. (C) Training time (in hours) comparison between MBN and DBN.

spectral clustering [5], and t-SNE [9]. The competitive methods are all one-layer nonlinear dimension reduction methods. The parameters of Isomap and LLE (i.e., the number of the neighbors of each data point) were searched from 2 to 20. The parameter of spectral clustering (i.e., the kernel width of the Gaussian kernel) was searched through  $\{2^{-3}A, 2^{-2}A, \dots, 2^3A\}$  where  $A$  was the average pairwise Euclidean distance between the data points. The parameters of t-SNE were the same as the authors' default setting [9].

We ran the experiment 10 times and reported the average performance. For each experimental running, we ran the  $k$ -means clustering on the entire data set 50 times and recorded the average accuracy values. The accuracy was measured by NMI [23], which was proposed to overcome the label indexing problem between the ground-truth labels and the predicted labels [23]. It is one of the standard evaluation metrics of clustering.

#### E. Experimental Details on Small Subsets of MNIST Digits

The data set of the MNIST handwritten digits [47] contains 10 hand written integer digits ranging from 0 to 9. It consists of 60,000 training images and 10,000 test images. Each image has 784 dimensions. The largest value

and smallest value of MNIST are 255 and 0 respectively. We constructed 5 small subsets from MNIST. Each subset consists of 5,000 randomly sampled images with 500 images per digit. We normalized each image to the range  $[0, 1]$  by dividing each entry of the image by 255. To our knowledge, t-SNE achieved the state-of-the-art performance on small subsets of MNIST [9].

The parameter setting of MBN was as follows. The number of hidden layers was set to 9. Parameters  $k$  from layer 1 to layer 9 were set to 4000-2000-1000-500-250-125-65-30-15 respectively. Parameter  $V$  was set to 2000 for all layers. Parameter  $a$  was set to 0.5. Parameter  $r$  was set to 0.5. The output dimension of EM-PCA was selected from  $\{2, 3, 5, 10, 20, 30\}$ . Euclidean distance was used as the similarity measurement of the bottom layer.

We compared MBN with PCA, Isomap [3], LLE [4], spectral clustering [5], t-SNE [9], and DBN [12]. The parameter settings of the competitive methods were as follows. The parameters of Isomap and LLE (i.e., the number of the neighbors of each data point) were searched from 2 to 20. The parameter of spectral clustering (i.e., the kernel width of the Gaussian kernel) was searched through  $\{2^{-3}A, 2^{-2}A, \dots, 2^3A\}$  where  $A$  was the average pairwise Euclidean distance between the data points. The parameter setting of DBN was the same as the authors' default setting [12] except that the output dimension of the linear output layer was selected from  $\{2, 3, 5, 10, 20, 30\}$ . For t-SNE, when the target dimension was lower than 30, the output dimension of PCA in the initialization stage of t-SNE was set to 30 which was the author's default setting; when the target dimension was 30, the output dimension of PCA was set to 60; other parameters were the same as the authors' default setting [9].

We used the low-dimensional features for visualization and clustering. For clustering, we ran the  $k$ -means clustering on the  $\{2, 3, 5, 10, 20, 30\}$ -dimensional features respectively 10 times and recorded the average accuracies on each dimension. The reported accuracies were average ones over all 5 small subsets of MNIST.

#### F. Experimental Details on the MNIST Digits

The data set of the MNIST handwritten digits [47] contains 10 hand written integer digits ranging from 0 to 9. It consists of 60,000 training images and 10,000 test images. Each image has 784 dimensions. The largest value and smallest value of MNIST are 255 and 0 respectively. We normalized each image to the range  $[0, 1]$  by dividing each entry of the image by 255.

The parameter setting of MBN was as follows. The number of hidden layers was set to 7. Parameters  $k$  from layer 1 to layer 7 were set to 1000-500-250-125-65-30-15 respectively. Parameter  $V$  was set to 400 for all layers. Parameter  $a$  was set to 0.5. Parameter  $r$  was set to 0. The output dimension of EM-PCA was selected from  $\{2, 3, 5, 10\}$ . Euclidean distance was used as the similarity measurement of the bottom layer.

We compared MBN with PCA and DBN [12]. The parameter setting of DBN was the same the authors' default

setting [12] except that the output dimension of the linear output layer was selected from  $\{2, 3, 5, 10\}$ .

We used the 60,000 training images to train the models, and evaluated the effectiveness of the low-dimensional features of the 10,000 test images by the  $k$ -means clustering. NMI was used as the evaluation metric of accuracy. The reported accuracies were average ones over the results of 10 independent runs of the  $k$ -means clustering.

#### G. Experimental Details on the Reuters Newswire Stories

The data set of Reuters newswire stories [49], [56] consists of 804,414 documents, which are divided into 103 topics. Because the topics are grouped into a tree structure, we only preserved the leaf topics. Finally, the 804,414 documents were divided to 82 topics. There were 107,132 unlabeled documents in this setting. We first preprocessed each document as a vector of 2,000 commonest word stems by the *rainbow* software [57], where each entry of the vector was the word count. Other parameters of rainbow were set to their default values. Then, we normalized each vector by dividing each entry of the vector by the maximal value of the vector.

The parameter setting of MBN was as follows. The number of hidden layers was set to 6. Parameters  $k$  from layer 1 to layer 6 were set to 500-250-125-65-30-15 respectively. Parameter  $V$  was set to 200. Parameter  $a$  was set to 0.5. Parameter  $r$  was set to 0. The output dimension of EM-PCA was 5. The similarity measurement at the bottom layer was the same as the other hidden layers.

We compared MBN with LSA [48] and DBN [12]. Because we could not follow exactly the experiment of DBN on this data set [12], we only reproduced its running time.

We randomly selected half of the data set for training and the other half for test. We tested the average accuracy over all 402,207 queries on the test set at the document retrieval setting, where each query was a document in the test set. The similarity between any two five-dimensional features was measured by the Euclidean distance. If the unlabeled documents were retrieved, they were considered as mistakes. If the unlabeled documents were used as queries, no relevant documents would be retrieved, which means the precisions of the unlabeled queries were zero at all levels. Because the accuracy curves of layers 5 and 6 were similar with the accuracy curve of layer 4, we only reported the accuracy curves of the bottom 4 layers in Fig. 5B. Different from the aforementioned parameter setting of MBN, the visualization in Fig. 5A was produced by the MBN with the random reconstruction, i.e.,  $r = 0.5$ . Empirical results showed that the two-dimensional visualization with  $r = 0.5$  was more compact than the visualization with  $r = 0$ ; however, when using the two-dimensional features for document retrieval, they achieved similar performance.

#### H. How does parameter $V$ affect the performance?

Parameter  $V$  represents the number of clusterings in each layer. We first analyzed  $V$  on the MNIST digits. Parameter



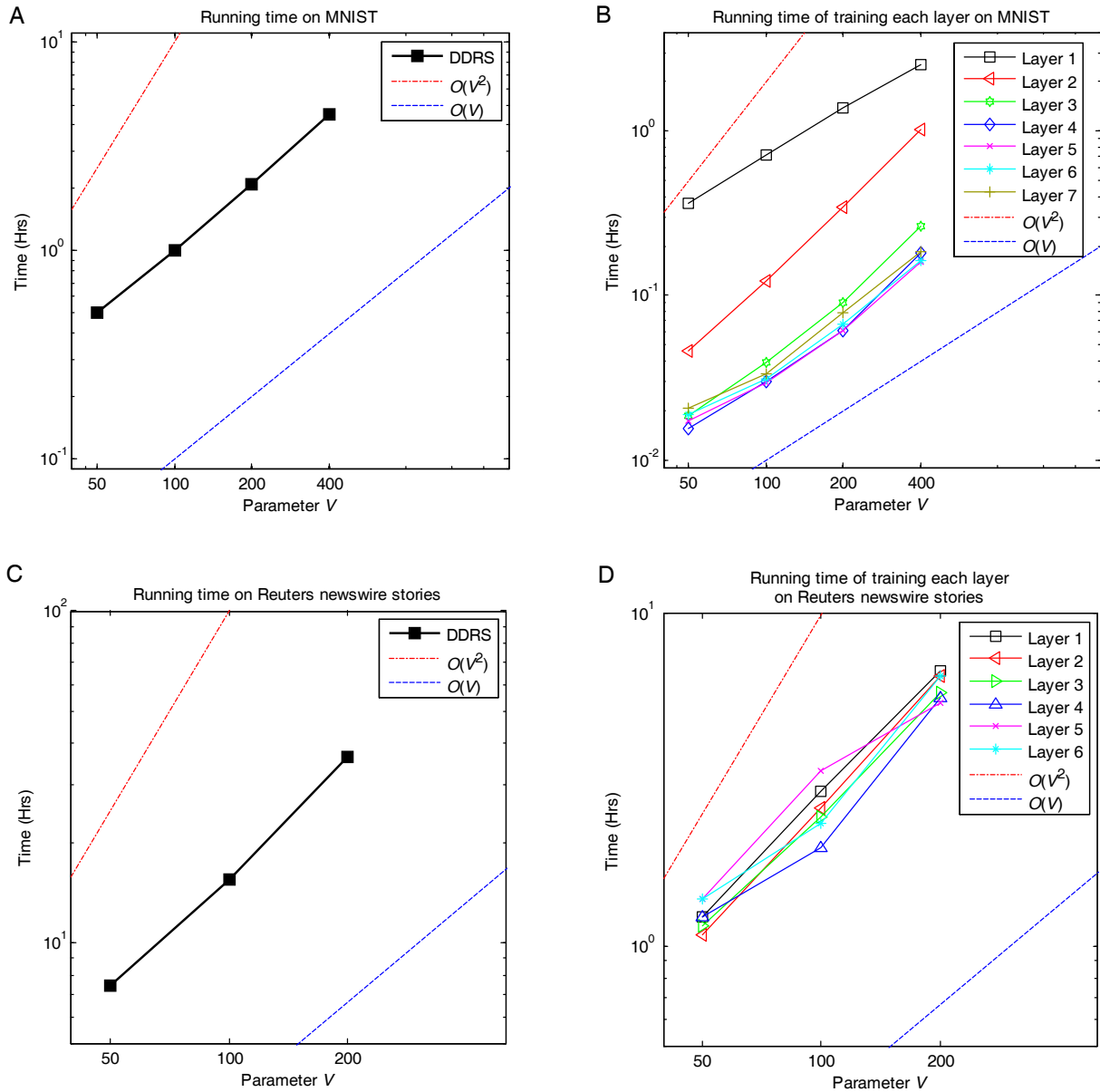


Fig. 6. Time complexity analysis on parameter  $V$  of MBN. (A) Curve of the CPU time (in hours) on MNIST. (B) Curves of the CPU time (in hours) consumed on training different hidden layers on MNIST. (C) Curve of the CPU time (in hours) on the Reuters newswire stories. (D) Curves of the CPU time (in hours) consumed on training different hidden layers on the Reuters newswire stories.

$V$  was selected from  $\{50, 100, 200, 400, 800\}$ . Other parameters were set as follows. The number of hidden layers was set to 7. Parameters  $k$  from layer 1 to layer 7 were set to 1000-500-250-125-65-30-15 respectively. Parameter  $a$  was set to 0.5. Parameter  $r$  was set to 0. The output dimension of EM-PCA was selected from  $\{2, 3, 5, 10, 20, 30\}$ . Euclidean distance was used as the similarity measurement of the bottom layer.

The accuracy curves of the  $k$ -means clusterings with different  $V$  of MBN are shown in Fig. 7. From the figure, we observed that setting  $V = 100$  achieved reasonable accuracy curves in most cases, and setting  $V$  to relatively larger values continued to achieve slightly better accuracy curves.

The running time of MBN with different  $V$  on MNIST

are shown in Fig. 6A. From the figure, we found that the time complexity scaled linearly but not squaredly with  $V$ , which conflicted with our theoretical conclusion on the time complexity of MBN. Hence, we further drew the running time of MBN on training each layer in Fig. 6B. From the figure, we found that training the bottom layer was the most time-consuming part which consumed 80% of the total running time when  $V = 50$  and 50% of the total running time when  $V = 400$ . We also recorded the total running time of MBN and the running time of MBN on training each layer on the Reuters newswire stories in Fig. 6C and Fig. 6D, respectively. From the figures, we found that the running time scaled linearly with  $V$  too, though the running time on training the bottom layer did not dominate the total running time.

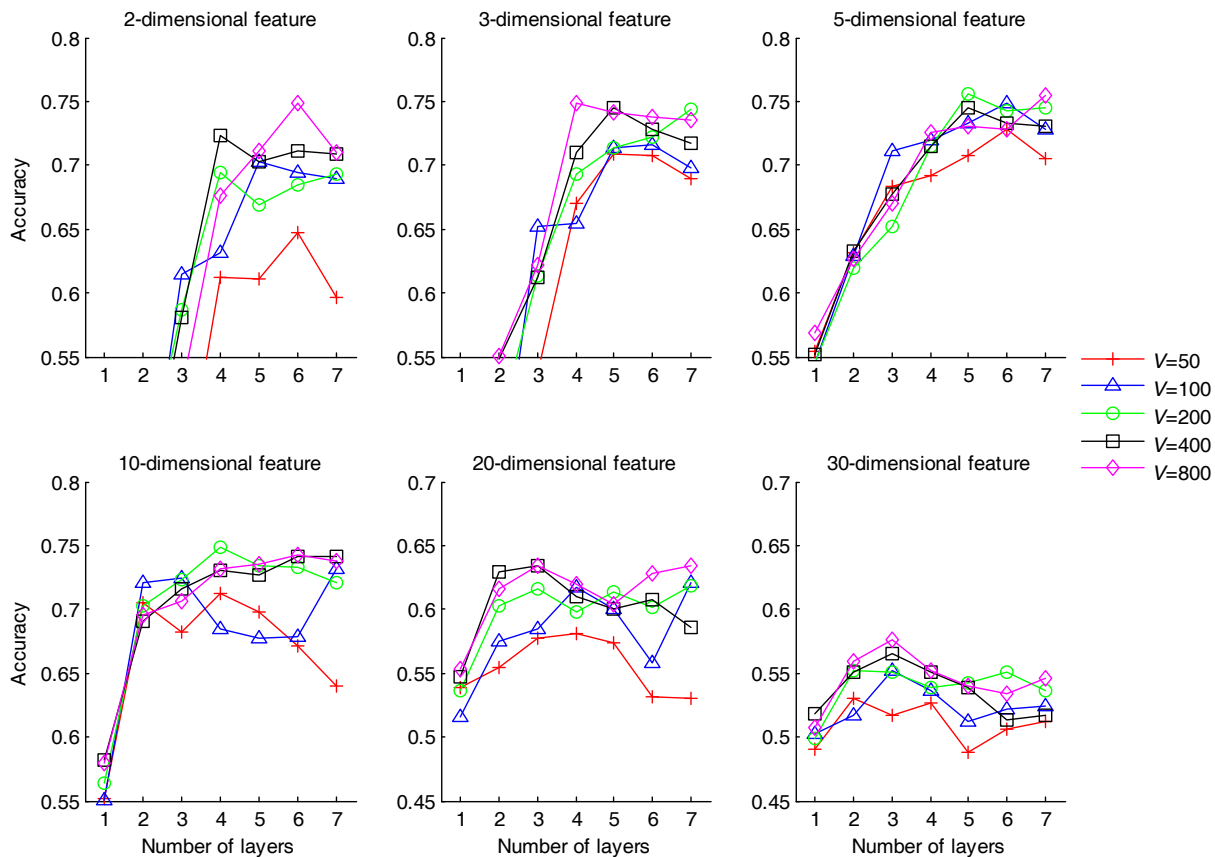


Fig. 7. Performance analysis on parameter  $V$  of MBN on the MNIST handwritten digits.

Summarizing the above experimental phenomena, we can only explain the reason why the empirical time complexity scaled linearly but not squaredly with  $V$  as that the input data was sparse. Specifically, the multiplication operation of two sparse matrices only considers the element-wise multiplication of two elements that are both nonzero, so that when the input data is sparse, one factor  $V$  in the equation of time complexity is offset by the sparsity factor  $s$ .

#### I. How does parameter $a$ affect the accuracy?

Parameter  $a$  represents the fraction of the randomly selected features over all input features. This parameter is used to enhance the *diversity* between the base clusterings, where the word “diversity” means when the base clusterings make predictions on an identical pattern, they are different from each other in terms of errors.

We analyzed parameter  $a$  on MNIST. Parameter  $a$  was selected from  $\{0.5, 0.6, 0.7, 0.8, 0.9, 1.0\}$ . Other parameters were set as follows. The number of hidden layers was set to 7. Parameter  $V$  was set to 400. Parameters  $k$  from layer 1 to layer 7 were set to 1000-500-250-125-65-30-15 respectively. Parameter  $r$  was set to 0. The output dimension of EM-PCA was selected from  $\{2, 3, 5, 10, 20, 30\}$ . Euclidean distance was used as the similarity measurement of the bottom layer.

The accuracy curves of the  $k$ -means clusterings with different  $a$  of MBN are shown in Fig. 8. From the figure, we observed that parameter  $a$  did not have an important impact on the accuracy curves. However, smaller  $a$  means less computational load and less memory requirement.

#### J. How do parameters $k$ and $r$ affect the accuracy?

Parameter  $k$  represents the number of the output units of each  $k$ -centers clustering. Parameter  $r$  represents the fraction of the randomly shifted features over all features of the centers in the reconstruction operation. Because  $k$  and  $r$  have a strong correlation, we analyzed them jointly.

When the data set is large-scale,  $k$  is usually much smaller than the size of the data set. We studied this situation on MNIST. Parameter  $r$  was selected from  $\{0.0, 0.1, 0.2, 0.3, 0.4, 0.5\}$ . Other parameters were set as follows. Parameters  $k$  from layer 1 to layer 7 were set to 1000-500-250-125-65-30-15 respectively. Parameter  $V$  was set to 400. Parameter  $a$  was set to 0.5. The output dimension of EM-PCA was selected from  $\{2, 3, 5, 10, 20, 30\}$ . Euclidean distance was used as the similarity measurement of the bottom layer.

The accuracy curves of the  $k$ -means clusterings with different  $r$  of MBN on the MNIST image digits are shown in Fig. 9. From the figure, we observed that (i) the accuracy curves did not vary much with different  $r$  when the dimension was restricted to 2 to 5; (ii) the accuracy curves

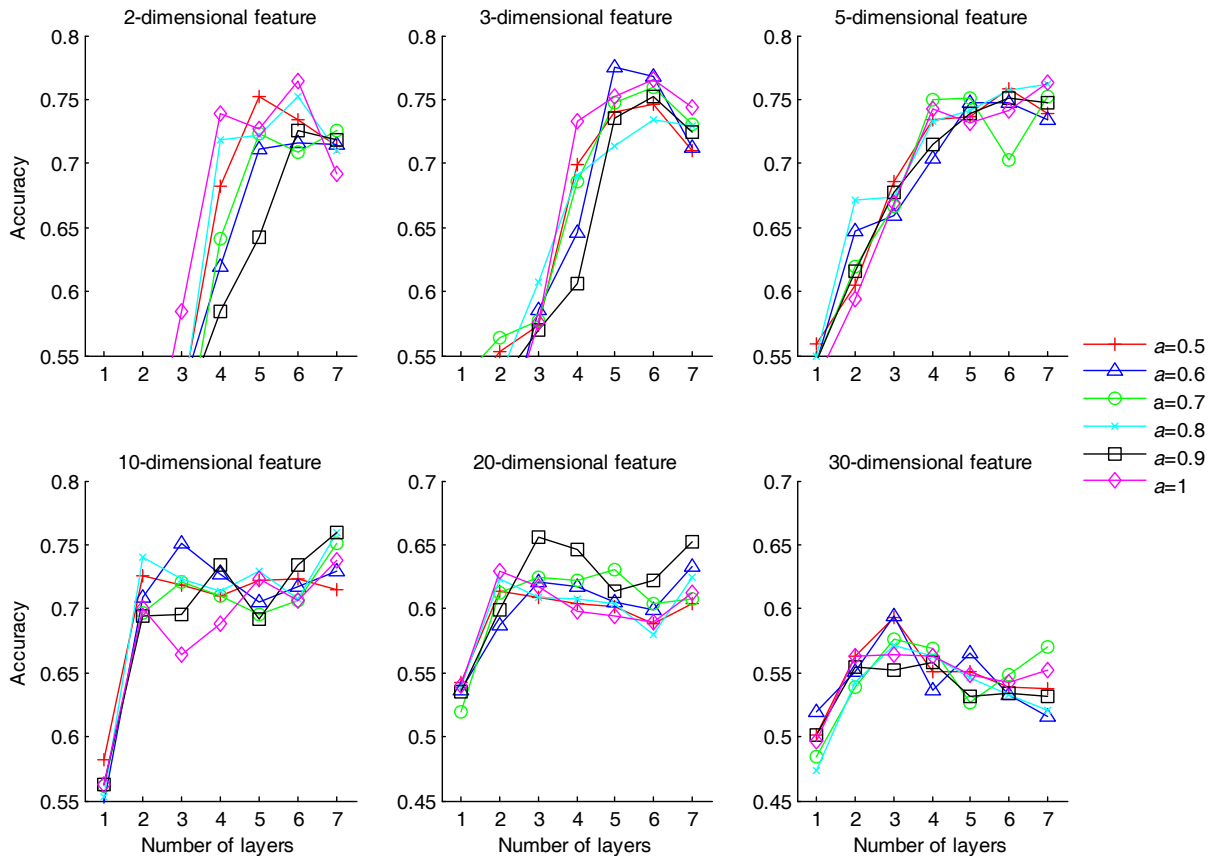


Fig. 8. Performance analysis on parameter  $a$  of MBN on the MNIST handwritten digits.

dropped along with the increase of  $r$ 's value when the dimension was enlarged to 10 to 30; (iii) the accuracy curves dropped more and more rapidly along with the increase of  $r$ 's value when the dimension was gradually enlarged from 5 to 30. Because using random reconstruction did not improve the performance, and was even harmful to the performance when the reduced dimension was large, as a conclusion, we should not use the random reconstruction operation for large-scale problems.

When the data set is small-scale,  $k$  is usually close to the size of the data set. We studied this situation on the small-scale AML-ALL biomedical data. Parameter  $r$  was selected from  $\{0.0, 0.5\}$ . Parameters  $k$  from layer 1 to layer 4 were set to 30-15-8-4 respectively. We further varied  $V$  from  $\{50, 400, 2000\}$ . Parameter  $a$  was set to 0.5. The output dimension of the linear-kernel-based kernel-PCA was selected from  $\{2, 3, 5, 10\}$ . Euclidean distance was used as the similarity measurement of the bottom layer.

The accuracy curves of the  $k$ -means clusterings with different  $r$  of MBN on the AML-ALL biomedical data are shown in Fig. 10. From the figure, we observed that no matter what value parameter  $V$  was set to, the accuracy curves of MBN with the random reconstruction (i.e.,  $r = 0.5$ ) were apparently better than those without the random reconstruction (i.e.,  $r = 0.0$ ). As a conclusion, we should use the random reconstruction operation for small-scale problems, otherwise, the performance will drop

significantly.

#### ACKNOWLEDGEMENT

The author thanks Prof. DeLiang Wang for providing the Ohio Supercomputing Center, Columbus, OH, USA for the empirical study.

#### REFERENCES

- [1] B. Schölkopf, A. Smola, and K.-R. Müller, "Nonlinear component analysis as a kernel eigenvalue problem," *Neural Comput.*, vol. 10, no. 5, pp. 1299–1319, 1998.
- [2] J. Shi and J. Malik, "Normalized cuts and image segmentation," *IEEE Trans. Pattern Anal. Machine Intell.*, vol. 22, no. 8, pp. 888–905, 2000.
- [3] J. B. Tenenbaum, V. De Silva, and J. C. Langford, "A global geometric framework for nonlinear dimensionality reduction," *Science*, vol. 290, no. 5500, pp. 2319–2323, 2000.
- [4] S. T. Roweis and L. K. Saul, "Nonlinear dimensionality reduction by locally linear embedding," *Science*, vol. 290, no. 5500, pp. 2323–2326, 2000.
- [5] A. Y. Ng, M. I. Jordan, and Y. Weiss, "On spectral clustering: Analysis and an algorithm," in *Advances in Neural Information Processing Systems 14*, Vancouver, British Columbia, Canada, 2002, pp. 849–856.
- [6] M. Belkin and P. Niyogi, "Laplacian eigenmaps for dimensionality reduction and data representation," *Neural Comput.*, vol. 15, no. 6, pp. 1373–1396, 2003.
- [7] X. He and X. Niyogi, "Locality preserving projections," in *Advances in Neural Information Processing Systems 17*, vol. 16, Vancouver, British Columbia, Canada, 2004, pp. 153–160.
- [8] S. Yan, D. Xu, B. Zhang, H.-J. Zhang, Q. Yang, and S. Lin, "Graph embedding and extensions: a general framework for dimensionality reduction," *IEEE Trans. Pattern Anal. Machine Intell.*, vol. 29, no. 1, pp. 40–51, 2007.

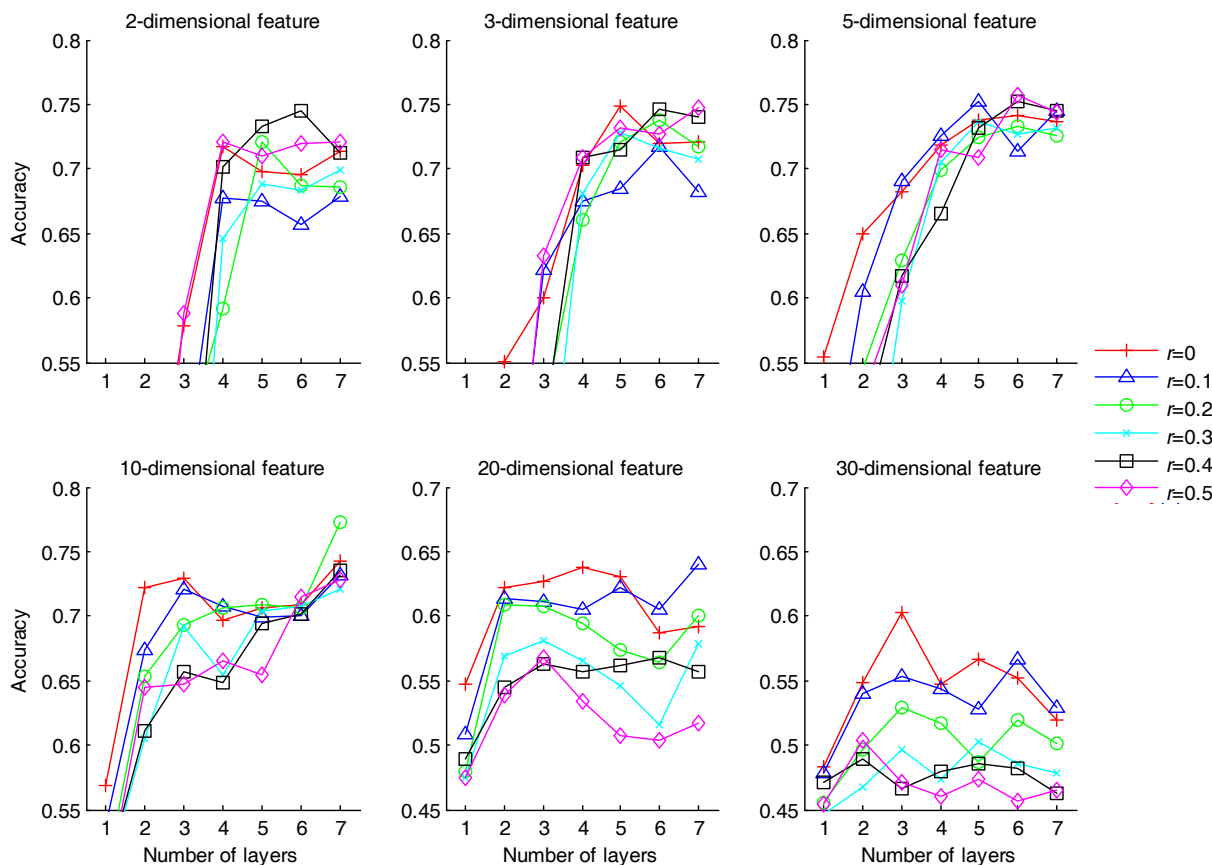


Fig. 9. Performance analysis on parameter  $r$  of MBN on the MNIST handwritten digits.

- [9] L. Van der Maaten and G. Hinton, "Visualizing data using t-sne," *J. Mach. Learn. Res.*, vol. 9, no. 85, pp. 2579–2605, 2008.
- [10] J. J. Hopfield, "Neural networks and physical systems with emergent collective computational abilities," *Proc. Natl. Acad. Sci. U.S.A.*, vol. 79, no. 8, pp. 2554–2558, 1982.
- [11] D. E. Rumelhart, G. E. Hinton, and R. J. Williams, "Learning representations by back-propagating errors," *Nature*, vol. 323, no. 6088, pp. 533–536, 1986.
- [12] G. E. Hinton and R. R. Salakhutdinov, "Reducing the dimensionality of data with neural networks," *Science*, vol. 313, no. 5786, pp. 504–507, 2006.
- [13] T. Hofmann, "Probabilistic latent semantic indexing," in *Proc. 22nd Int. ACM SIGIR Conf. Res. Dev. Inform. Retrieval*. ACM, 1999, pp. 50–57.
- [14] D. M. Blei, A. Y. Ng, and M. I. Jordan, "Latent dirichlet allocation," *J. Mach. Learn. Res.*, vol. 3, pp. 993–1022, 2003.
- [15] G. E. Hinton, S. Osindero, and Y.-W. Teh, "A fast learning algorithm for deep belief nets," *Neural Comput.*, vol. 18, no. 7, pp. 1527–1554, 2006.
- [16] B. A. Olshausen and D. J. Field, "Emergence of simple-cell receptive field properties by learning a sparse code for natural images," *Nature*, vol. 381, no. 6583, pp. 607–609, 1996.
- [17] L. Van der Maaten, E. Postma, and H. Van Den Herik, "Dimensionality reduction: A comparative review," *J. Mach. Learn. Res.*, vol. 10, pp. 1–41, 2009.
- [18] C. Sorzano, J. Vargas, and A. P. Montano, "A survey of dimensionality reduction techniques," *arXiv preprint arXiv:1403.2877*, pp. 1–35, 2014.
- [19] B. Efron, "Bootstrap methods: another look at the jackknife," *Ann. Stat.*, vol. 7, no. 1, pp. 1–26, 1979.
- [20] B. Efron and R. Tibshirani, *An Introduction to the Bootstrap*. CRC press, 1993.
- [21] Y. Freund and R. E. Schapire, "A decision-theoretic generalization of on-line learning and an application to boosting," in *Proceedings of the 2nd European Conference on Computational Learning Theory*, Barcelona, Spain, 1995, pp. 23–37.
- [22] L. Breiman, "Random forests," *Machine Learn.*, vol. 45, no. 1, pp. 5–32, 2001.
- [23] A. Strehl and J. Ghosh, "Cluster ensembles—a knowledge reuse framework for combining multiple partitions," *J. Mach. Learn. Res.*, vol. 3, pp. 583–617, 2003.
- [24] A. L. Fred and A. K. Jain, "Combining multiple clusterings using evidence accumulation," *IEEE Trans. Pattern Anal. Machine Intell.*, vol. 27, no. 6, pp. 835–850, 2005.
- [25] S. Vega-Pons and J. Ruiz-Shulcloper, "A survey of clustering ensemble algorithms," *Int. J. Pattern Recogn. Artif. Intell.*, vol. 25, no. 03, pp. 337–372, 2011.
- [26] J. H. Holland, *Adaptation in Natural and Artificial Systems: An Introductory Analysis with Applications to Biology, Control, and Artificial Intelligence*. U Michigan Press, 1975.
- [27] L. Breiman, "Bagging predictors," *Machine Learn.*, vol. 24, no. 2, pp. 123–140, 1996.
- [28] R. E. Schapire, "The strength of weak learnability," *Machine Learn.*, vol. 5, no. 2, pp. 197–227, 1990.
- [29] T. G. Dietterich and G. Bakiri, "Solving multiclass learning problems via error-correcting output codes," *J. Artif. Intell. Res.*, vol. 2, pp. 263–286, 1995.
- [30] T. G. Dietterich, "Ensemble methods in machine learning," *Multiple Classifier Systems*, pp. 1–15, 2000.
- [31] Z.-H. Zhou, J. Wu, and W. Tang, "Ensembling neural networks: many could be better than all," *Artif. Intell.*, vol. 137, no. 1, pp. 239–263, 2002.
- [32] Z.-H. Zhou, *Ensemble Methods: Foundations and Algorithms*. CRC Press, 2012.
- [33] A. Tikhonov, "Solution of incorrectly formulated problems and the regularization method," *Soviet Math. Dokl.*, vol. 5, pp. 1035–1038, 1963.
- [34] T. Poggio and F. Girosi, "Networks for approximation and learning," *Proc. IEEE*, vol. 78, no. 9, pp. 1481–1497, 1990.
- [35] —, "Regularization algorithms for learning that are equivalent to multilayer networks," *Science*, vol. 247, no. 4945, pp. 978–982, 1990.

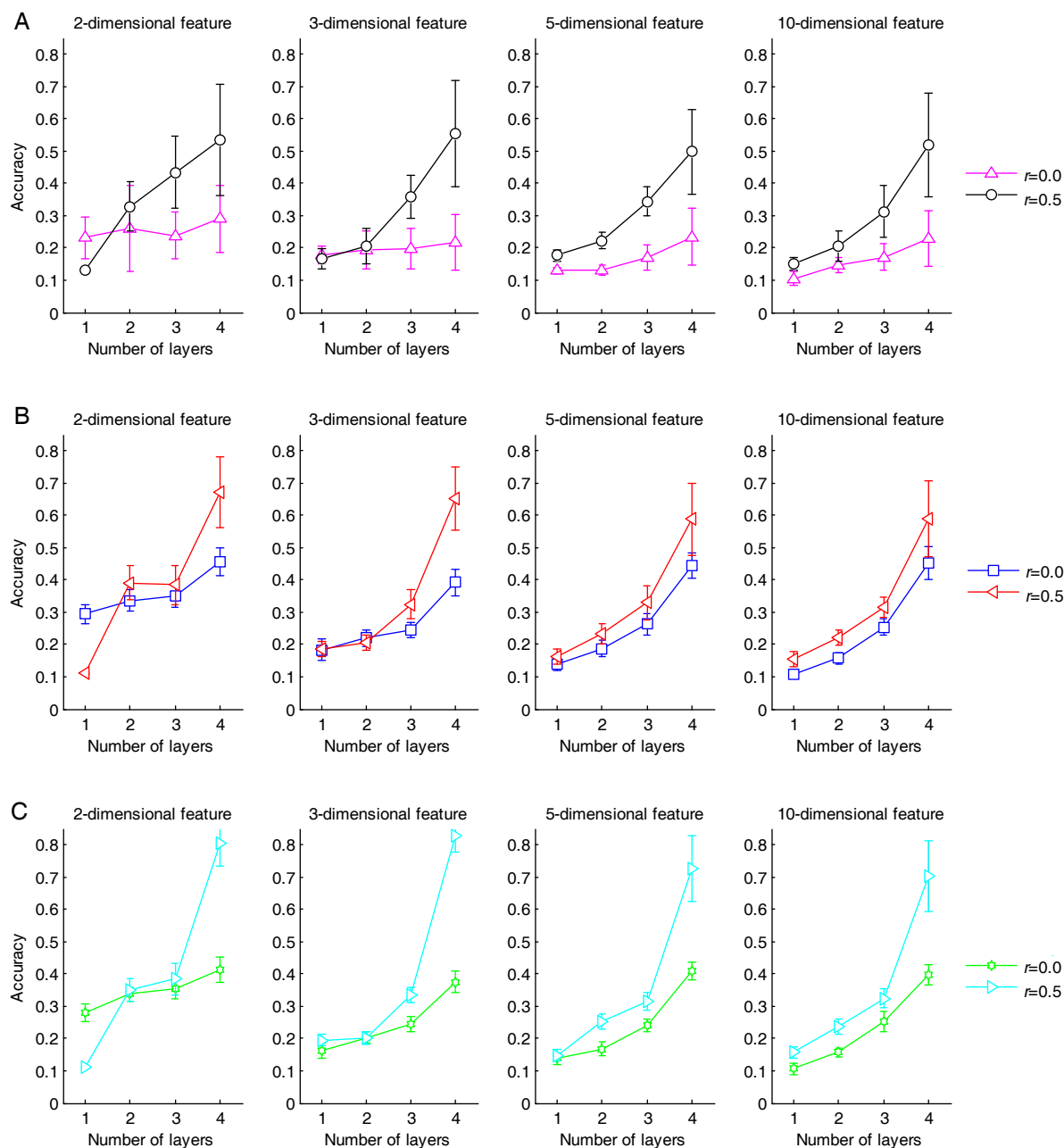


Fig. 10. Performance analysis on parameter  $r$  of MBN on the AML-ALL biomedical data. (A) Accuracy curves of the  $k$ -means clusterings when parameter  $V$  was set to 50. (B) Accuracy curves when parameter  $V$  was set to 400. (C) Accuracy curves when parameter  $V$  was set to 2000.

- [36] R. E. Schapire, Y. Freund, P. Bartlett, and W. S. Lee, "Boosting the margin: A new explanation for the effectiveness of voting methods," *Ann. Stat.*, vol. 26, no. 5, pp. 1651–1686, 1998.
- [37] C. Cortes and V. Vapnik, "Support-vector networks," *Machine Learn.*, vol. 20, no. 3, pp. 273–297, 1995.
- [38] V. N. Vapnik, *Statistical Learning Theory*. Wiley, 1998.
- [39] G. E. Hinton, "Products of experts," in *Proceedings of the 9th International Conference on Artificial Neural Networks*, Edinburgh, United Kingdom, 1999, pp. 1–6.
- [40] —, "Training products of experts by minimizing contrastive divergence," *Neural Comput.*, vol. 14, no. 8, pp. 1771–1800, 2002.
- [41] A. Coates and A. Ng, "The importance of encoding versus training with sparse coding and vector quantization," in *Proceedings of the 28th International Conference on Machine Learning*, Bellevue, Washington, 2011, pp. 921–928.
- [42] Y. Bengio, "Learning deep architectures for AI," *Foundations and Trends® in Machine Learning*, vol. 2, no. 1, pp. 1–127, 2009.
- [43] C. M. Bishop *et al.*, *Pattern Recognition and Machine Learning*. Springer New York, 2006.
- [44] C. Andrieu, N. De Freitas, A. Doucet, and M. I. Jordan, "An introduction to MCMC for machine learning," *Maching Learn.*, vol. 50, no. 1, pp. 5–43, 2003.
- [45] S. P. Boyd and L. Vandenberghe, *Convex Optimization*. Cambridge University Press, 2004.
- [46] T. R. Golub, D. K. Slonim, P. Tamayo, C. Huard, M. Gaasenbeek, J. P. Mesirov, H. Coller, M. L. Loh, J. R. Downing, M. A. Caligiuri *et al.*, "Molecular classification of cancer: class discovery and class prediction by gene expression monitoring," *Science*, vol. 286, no. 5439, pp. 531–537, 1999.
- [47] Y. Lecun, C. Cortes, and C. J. C. Burges, "THE MNIST DATABASE of handwritten digits," <http://yann.lecun.com/exdb/mnist/index.html>, 2004.
- [48] S. C. Deerwester, S. T. Dumais, T. K. Landauer, G. W. Furnas, and R. A. Harshman, "Indexing by latent semantic analysis," *J. Am. Soc.*

- Inf. Sci.*, vol. 41, no. 6, pp. 391–407, 1990.
- [49] D. D. Lewis, Y. Yang, T. G. Rose, and F. Li, “RCV1: a new benchmark collection for text categorization research,” *J. Mach. Learn. Res.*, vol. 5, pp. 361–397, 2004.
- [50] B. Schölkopf and A. J. Smola, *Learning With Kernels*. The MIT Press, 2002.
- [51] B. Schölkopf, A. Smola, and K.-R. Müller, “Kernel principal component analysis,” in *Proceedings of the 7th International Conference on Artificial Neural Networks*, Lausanne, Switzerland, 1997, pp. 583–588.
- [52] S. Canu, Y. Grandvalet, V. Guigue, and A. Rakotomamonjy, “SVM and kernel methods Matlab toolbox,” <http://asi.insa-rouen.fr/enseignants/~arakoto/toolbox/index.html>, 2005.
- [53] S. T. Roweis, “EM algorithms for PCA and SPCA,” in *Advances in Neural Information Processing Systems 10*, Denver, CO, 1998, pp. 626–632.
- [54] M. Brookes, “VOICEBOX: Speech Processing Toolbox for MATLAB,” <http://www.ee.ic.ac.uk/hp/staff/dmb/voicebox/voicebox.html>, 2003.
- [55] T. R. Golub, D. K. Slonim, P. Tamayo, C. Huard, M. Gaasenbeek, J. P. Mesirov, H. Coller, M. L. Loh, J. R. Downing, M. A. Caligiuri *et al.*, “Molecular classification of cancer: class discovery and class prediction by gene expression monitoring,” [http://www.broadinstitute.org/cgi-bin/cancer/publications/pub\\_paper.cgi?mode=view&paper\\_id=43](http://www.broadinstitute.org/cgi-bin/cancer/publications/pub_paper.cgi?mode=view&paper_id=43), pp. 531–537, 1999.
- [56] D. D. Lewis, “RCV1-v2/LYRL2004: The LYRL2004 Distribution of the RCV1-v2 Text Categorization Test Collection,” [http://www.ai.mit.edu/projects/jmlr/papers/volume5/lewis04a/lyrl2004\\_rcv1v2\\_README.htm](http://www.ai.mit.edu/projects/jmlr/papers/volume5/lewis04a/lyrl2004_rcv1v2_README.htm), 2004.
- [57] A. McCallum, “Rainbow,” <http://www.cs.cmu.edu/~mccallum/bow/rainbow>, 1998.